Quasiparticle scattering interference in iron pnictides: A probe of the origin of nematicity

Hai-Yang Zhang and Jian-Xin Li*
National Laboratory of Solid State Microstructure and Department of Physics, Nanjing University, Nanjing 210093, China
Collaborative Innovation Center of Advanced Microstructures, Nanjing University, Nanjing, China
(Dated: December 13, 2016)

In this paper, we investigate the quasiparticle scattering interference(QPI) in the nematic phase of iron pnictides, based on the magnetic and orbital scenarios of nematicity, respectively. In the spin density wave(SDW) state, the QPI pattern exhibits a dimer structure in the energy region of the SDW gap, with its orientation along the ferromagnetic direction of the SDW order. When the energy is increased to be near the Fermi level, it exhibits two sets of dimers along the same direction. The dimer structure of the QPI patterns persists in the magnetically driven nematic phase, although the two dimers tend to merge together with energies closing to the Fermi level. While in the orbital scenario, the QPI patterns exhibit a dimer structure in a wide energy region. It undergoes a $\pi/2$ rotation with the increasing of energy, which is associated with the inequivalent energies of the two Dirac nodes induced by the orbital order. These distinct features may be used to probe or distinguish two kinds of scenarios of the nematicity.

PACS numbers: 74.70.Xa, 72.10.Fk, 75.30.Fv, 75.25.Dk

arXiv:1603.02517v2 [cond-mat.str-el] 10 Dec 2016

I. INTRODUCTION

In recent years, the unconventional superconductivity found in iron-based superconductors(IBSCs) has attracted much attention in condensed matter community. Due to the proximity of superconductivity and the collinear spin density wave(SDW) phase, it is generally believed that there exists an intrinsic link between the magnetic fluctuations and the superconductivity. Thus, the understanding of the normal state magnetic fluctuations will be helpful to identify the mechanism of superconductivity. Experimentally, it was found that the SDW transition is either preemptive by or coincident with a tetragonal-to-orthorhombic(TO) structural transition at T_s[1–3] which signals the C_4 symmetry breaking above the SDW transition temperarture T_N. Such a C_4 symmetry breaking phase is called the nematic phase in literatures[4]. Further studies show that the nematicity persists to T^* above T_s[5–8]. So far, there is clear evidence that nematicity comes from the electronic rather than the lattice degree of freedom[9,10]. However, it is difficult to identify the fingerprint of nematicity due to the coupling of various electronic degrees of freedom. Experimentally, it was found that the presence of nematicity is accompanied by anisotropic magnetic correlations which indicates its magnetic origination[5,11]. Meanwhile, it was also found that the characteristic temperature T^* of nematicity coincides with that of the orbital order[6,12,13], which indicates that nematicity is orbitally driven. So, the origin of nematicity is still debated, both the magnetic and orbital fluctuations are proposed to be responsible for the emergence of nematicity[14–17]. Thus, the study of the origin of nematicity is highly desired as it may shed light on the mechanism of unconventional superconductivity in IBSCs.

One of the effective ways to distinguish between different scenarios of nematicity is to compare the theoretical results of each scenario to the experimental observations. In this regard, we notice that the electronic structure can be mapped effectively through the analysis of the quasiparticle scattering interference (QPI) patterns[18–21] and the spatial modulation of the electronic states resulting from QPI can be probed directly by the STM experiments. In fact, the recent STM experiments[22,23] for NaFeAs have been performed to investigate the electronic structure in the nematic phase in IBSCs. The STM experiments[22,23] reveal that the QPI patterns exhibit highly anisotropic dimer structure deep in the SDW phase. It was further found that the anisotropic features persist to high temperatures above T_s, but the anisotropy weakens gradually with the increase of temperature. Therefore, the QPI may offer a playground for the test of the origin of nematicity.

In this paper, we study theoretically the quasiparticle interference induced by impurity in the nematic phase based on the magnetic and orbital scenarios of nematicity, respectively. Deep in the collinear $(\pi, 0)$ SDW state, the low energy QPI patterns exhibit a dimer structure with its orientation along the ferromagnetic direction of the SDW state. This is due to the fully opening of the SDW gap along the k_x direction. When the energy is increased to be slightly below the Fermi level, it is composed of two sets of dimers along the same direction. In this case, the QPI reflects the topology of the distorted Fermi surface and the two sets of dimers come from the inter-hole-pocket and intra-hole-pocket scatterings. It is further shown that the above features of the QPI patterns remain in the magnetically driven nematic phase, which is modelled by the fluctuating short-range antiferromagnetic order. In the orbital scenario of nematicity, it is found that the scatterings of quasiparticles between Dirac cones dominate the QPI process. Due to the inequivalent energy positions of the two Dirac cones resulting from the C_4 symmetry breaking induced by the orbital

order, the dimer structure in the QPI patterns undergoes a $\pi/2$ rotation with increasing energy. The transition is irrespective of the momentum dependence of the orbital order, so long as the energy splitting between the d_{xz} and d_{yz} bands is fixed near the Dirac cones. We propose that these results can be used to distinguish the origin of the nematicity in various iron-based compounds.

As a preliminary comparison to available experiments, we note that the obtained anisotropic features of the scattering patterns and the orientation of the dimer in the magnetic scenario are qualitatively consistent with the experimental observations on NaFeAs[22,23].

II. MODEL AND FORMULAS

The Hamiltonian we use to carry out the calculations can be divided into three parts: the tight binding part, the impurity part and that modelling the nematicity.

We adopt the five-orbital tight binding Hamiltonian of Ref[24] which reproduces the LDA energy bands. The tight binding Hamiltonian reads $H_0 = \sum_{k,a,b,\sigma} \epsilon_{ab}(k) C^+_{a\sigma}(k) C_{b\sigma}(k)$. Where a, b and σ are the orbital and spin indices, respectively. The tight binding hopping parameters for $\epsilon_{ab}(k)$ are given in Ref[24] and the energy unit eV will be used throughout the paper. In this paper, we focus on the QPI phenomenon induced by impurity potential scattering. The impurity Hamiltonian can be written as $H_{imp} = V_{ab} C^+_{i_0 a\sigma} C_{i_0 b\sigma}$. For simplicity, we adopt a δ-function type scattering potential which resides on the given lattice site i_0. The scattering matrix $V_{ab}(k, k+q) = V\delta_{ab}$ is orbital diagonal and momentum independent. In this paper, the average electron occupation number is fixed to be 6.0 per unit cell which corresponds to the undoped parent compound.

A. Modelling of the SDW state

In order to model the SDW and the magnetically driven nematic phase, we include the Coulomb interaction Hamiltonian. So, the full Hamiltonian reads $H_m = H_0 + H_{imp} + H_{int}$, and H_{int} is given by,

$$\begin{aligned} H_{int} = & U \sum_{i,a} n_{ia\uparrow} n_{ia\downarrow} + U^{'} \sum_{i,a<b} n_{ia} n_{ib} \\ & + J \sum_{i,a<b} C^+_{ia\sigma} C^+_{ib\sigma'} C_{ia\sigma'} C_{ib\sigma} \\ & + J^{'} \sum_{i,a\neq b} C^+_{ia\uparrow} C^+_{ia\downarrow} C_{ib\downarrow} C_{ib\uparrow}, \end{aligned} \tag{1}$$

Where a and b are the orbital indices. U, U', J, J' are the coefficients of the intraorbital interaction, interorbital interaction, Hund-coupling, and pair hopping terms, respectively. $U = U^{'} + J + J^{'}$ and $J = J^{'}$ are assumed as required by the spatial rotational symmetry. Without loss of generality, $J = U/4$ is assumed. H_{int} is treated at the mean field level, and is decoupled into the orbital diagonal channel in the following way[25–27],

$$\begin{aligned} H_{int} \simeq & U \sum_{i,a,\sigma} \langle n_{ia\sigma} \rangle n_{ia\bar{\sigma}} + (U^{'} - \frac{J}{2}) \sum_{i,a\neq b} \langle n_{ia} \rangle n_{ib} \\ & - 2J \sum_{i,a\neq b} \langle \mathbf{S}^z_{ia} \rangle \mathbf{S}^z_{ib}. \end{aligned} \tag{2}$$

Where n_{ia} and $\mathbf{S}_{ia}$ are the electron number and spin operators at site i with orbital a, respectively.

The values of $\langle n_{ia\sigma} \rangle$ and the magnetic moment S_a which is defined via $\mathrm{S}_a = \frac{1}{N} \sum_i (-)^{i_x} \langle \mathbf{S}^z_{ia} \rangle$ for the $(\pi, 0)$ SDW state (N the number of lattice sites, i_x the x-coordinate of site i) are obtained through the self-consistent calculations. In this paper, the intraorbital interaction $U = 1.3$ is adopted, which is slightly above the critical value $U_c = 1.24$ for the appearance of SDW. The results for the magnetic moments are $\mathrm{S}_{xz} = 0.029$, $\mathrm{S}_{yz} = 0.071$, $\mathrm{S}_{x^2-y^2} = 0.024$, $\mathrm{S}_{xy} = 0.044$, and $\mathrm{S}_{3z^2-r^2} = 0.028$. In Eq.(2), we have ignored the orbital off-diagonal magnetic terms. In fact, we have checked numerically the effects of these off-diagonal terms. We find that the nonzero orbital off-diagonal SDW moments are $\mathrm{S}_{x^2-y^2,3z^2-r^2} = \mathrm{S}_{3z^2-r^2,x^2-y^2} = -0.017$, where $S_{a,b} = \frac{1}{2N} \sum_i (-)^{i_x} \langle C^+_{ia\alpha} \sigma^z_{\alpha\beta} C_{ib\beta} \rangle$. These SDW moments are smaller compared to their diagonal parts, $\mathrm{S}_{xz} = 0.034$, $\mathrm{S}_{yz} = 0.077$, $\mathrm{S}_{x^2-y^2} = 0.029$, $\mathrm{S}_{xy} = 0.05$, and $\mathrm{S}_{3z^2-r^2} = 0.032$. Furthermore, we have checked that the off-diagonal SDW orders have no qualitative influences on the behaviors of the QPI patterns in the SDW and spin driven nematic state. Here, we focus mainly on the QPI within the orbital diagonal SDW approximation in the following discussions.

Within the $(\pi, 0)$ ansatz of the SDW order, we introduce the annihilation operator with ten components as $\psi_{k\sigma} = (C_{ka\sigma}, C_{k+Qa\sigma})^T$, where $Q = (\pi, 0)$ is the SDW wave vector. In this way, the Green's function reads $G_{k\sigma}(\tau) = -\langle T \psi_{k\sigma}(\tau) \psi^+_{k\sigma}(0) \rangle$ in the SDW state, where T is the time-ordering operator.

B. Modelling of the spin and orbital driven nematicity

Experimentally, the nematicity in Fe-pnictides and Fe-chalcogenides has been shown to develop at a temperature above the SDW transition[5–8]. Therefore, the magnetically driven nematicity where the long-range SDW order is absent but the C_4 symmetry is broken by magnetic fluctuations has been proposed[14,15,17]. This phase is modelled by the short-range antiferromagnetic correlation, which is approximated by the Lee-Rice-Anderson formula[28]. In this way, the Green's function is written as $\tilde{G}^{-1}_k = i\omega_n - \hat{\epsilon}_k - \sum_q P_q \frac{\hat{\Delta}^2}{i\omega_n - \hat{\epsilon}_{k+q+Q}}$, where $\hat{\epsilon}_k$ and $\hat{\epsilon}_{k+q+Q}$ are the matrix representation of the mean-field Hamiltonian H_m without the SDW terms. $P_q = \frac{1}{\xi^{-2} + q^2}$ is a Lorentzian which represents the q modulated magnetic correlation with ξ the correlation length and q

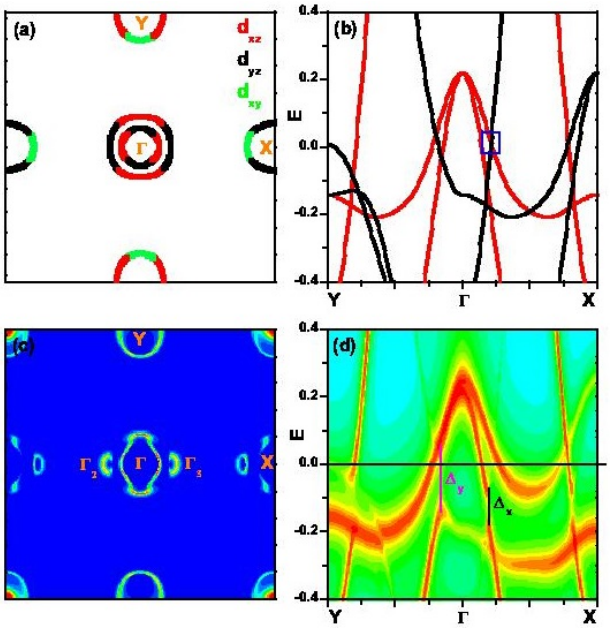

FIG. 1. (Color online) SDW distorted electronic structure. (a) The normal state Fermi surface and its dominate orbital components without the SDW order. (b) The red and black lines denote the original bands and the folded bands by the SDW order with wave vector $(\pi, 0)$, respectively. The blue square marks the location of the Dirac node in the momentum space. (c) The intensity map of the SDW distorted Fermi surface. Γ_2 and Γ_3 are two Dirac pockets. (d) The intensity map of the single-particle spectral function along the high symmetry directions. The intensity is in logarithmic scale in this panel.

the momenta derivation from $(\pi, 0)$. The orbital diagonal $\hat{\Delta}$ is the order parameter matrix of the fluctuating magnetic order. The elements of $\hat{\Delta}$ read as $\hat{\Delta}_{aa} = (U - J)\mathrm{S}_a + J\sum_b \mathrm{S}_b$ and $\hat{\Delta}_{ab} = 0 (a \neq b)$. Where S_a is the magnetic moment of orbital a. Following the previous study[28], the mean-field SDW order parameters obtained at $T = 0$ are taken to be S_a.

In the orbital scenario, the orbital orders are used to model the orbitally driven nematicity as used before[16,29,30]. Generally, the Hamiltonian for the orbital orders can be written as $H_{orb} = \sum_{ij,ab,\sigma} \lambda_{ij,ab} C^+_{ia\sigma} C_{jb\sigma}$ which breaks the C_4 symmetry, where $\lambda_{ij,ab}$ are the order parameters. The value of $\lambda_{ij,ab}$ is determined by the ARPES data. Thus, the full Hamiltonian reads $H_r = H_0 + H_{orb} + H_{imp}$ for the orbital scenario of nematicity in the presence of the impurity scattering. Both the momentum dependent and the momentum independent orbital orders will be considered in the following.

With the Hamiltonians shown above, we can now construct the corresponding Green's functions. For the orbital scenario of nematicity, the Green's function can be defined in the orbital basis as $G_{ab}(\tau) = -\langle T C_{ka}(\tau) C^+_{kb}(0)\rangle$ which can be obtained directly from H_r.

C. Calculation method of the QPI

The quasiparticle interference occurs between the ingoing and scattered outgoing electrons by impurity. The resulting spatial modulation of the electronic states can be visualized directly by the STM experiments[18,19]. After a Fourier transformation, one can get its manifestation in the momentum space, i.e., the density of states in the momentum space $\rho_q(\omega)$. Thus, the features of the QPI patterns can be qualitatively understood by the analysis of the joint density of states of the initial and final states. Theoretically, $\rho_q(\omega)$ is expressed as $\rho_q(\omega) = -\frac{1}{\pi}\mathrm{Im}\sum_{k\sigma} \mathrm{Tr}(G_{k\sigma} T_{k\sigma,k+q\sigma} G_{k+q\sigma})$, where the T matrix reads $T_{k\sigma,k+q\sigma} = V_{k,k+q} + \sum_{k'} V_{k,k'} G_{k'\sigma} T_{k'\sigma,k+q\sigma}$. In each scenario, the corresponding Green's function G_k is used to calculate $\rho_q(\omega)$. A Born limited scattering potential of $V = 0.05$ is adopted. In this case, the QPI patterns are not disturbed by the impurity resonance states, thus they are directly related to the underlying bands structure.

III. NUMERICAL RESULTS

A. QPI patterns in the magnetic scenario of nematicity

Let us start with the discussion of the distortion in the energy bands due to the collinear $(\pi, 0)$ SDW order with its moment antiferromagnetically aligning along the x direction but ferromagnetically along the y direction. In Fig. 1, we show the normal state Fermi surface (FS) and the resulted FS after the introduction of the SDW order. Clearly, the normal state hole FS around $\Gamma = (0, 0)$ develops into three distinct hole pockets Γ, Γ_2 and Γ_3 in the presence of the SDW order which induces the hybridization between the hole pockets around Γ and the electron pocket around $X = (\pi, 0)$. As revealed by previous study[31], the two small hole pockets Γ_2 and Γ_3 exhibit Dirac cone like dispersions. These Dirac cone dispersions persist even when the off-diagonal SDW orders are taken into account. The SDW distorted FSs calculated here are in qualitative agreement with the ARPES observations[32–35]. At the same time, the similar distortion of the Fermi pocket at X occurs, while the Fermi pocket around Y is affected less, because the $(\pi, 0)$ SDW order is considered here. Quite similar SDW distorted Fermi surfaces have been obtained by the previous calculations[26,31,36] based on the five orbital model. Meanwhile, our results for the single-particle spectrum are fully consistent with the previous study[26], as shown in Fig 1(d).

Further analysis shows that the highly anisotropic FS induced by the SDW is related directly to the orbital characters of the normal state energy bands. As presented in Fig. 1(a), the normal state FS is dominated by the d_{xz}, d_{yz} and d_{xy} orbitals. The overlap between the Γ and X pockets are dominated by the d_{yz} orbital, as a re-

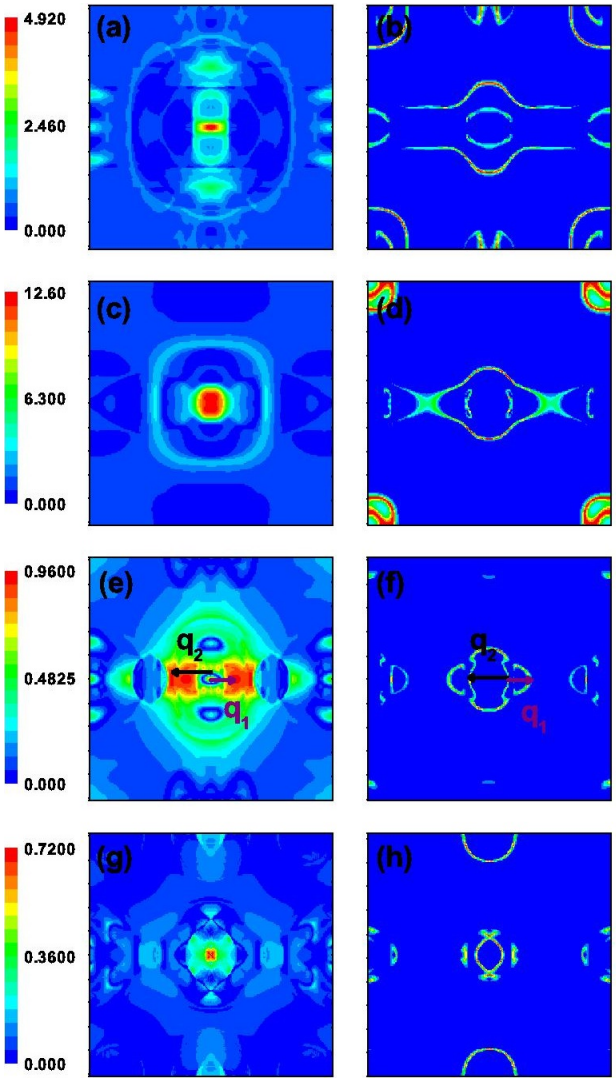

FIG. 2. (Color online) Energy evolution of the QPI patterns in the SDW state. Panels (a), (c), (e) and (g) are the QPI patterns at energies $\omega = -0.14$, -0.08, -0.04 and 0.08, respectively. The intensity maps of the corresponding quasiparticle spectral functions are plotted in the right side panels.

sult, their hybridization is maximum. Consequently, the coupling between the inner Γ pocket and the X pocket gives rise to a large SDW gap $\Delta_y \sim 0.19eV$ along k_y axis. On the other hand, the SDW gap $\Delta_x \sim 0.1eV$ along the k_x axis is smaller. This attributes to the fact that the overlap of the d_{xz} or d_{xy} band between the Γ pocket and the X pocket is weak. However, we note that the SDW gap opens along the full k_x axis, while only at individual k point along the k_y axis. In addition, the Dirac cone dispersions located at k_x axis are directly related to the orbital character of the relative bands[31]. Thus, the orbital degree of freedom plays an important role in the bands reconstruction in the SDW state.

Now, we study the energy evolution of the QPI patterns in the SDW state and the results are presented in Fig. 2. In Fig. 2(a), we show the QPI pattern for $\omega = -0.14$. Its main feature is obviously anisotropic with only C_2 symmetry and exhibits a dimer-like structure orienting along the q_y direction. We also show the intensity map of the corresponding quasiparticle spectral functions(QSFs) at the same energy in Fig. 2(b). One can see that the electronic states along the k_x axis are fully gapped, which is the consequence of the opening of the SDW gap Δ_x as can be seen from the single-particle spectrum presented in Fig. 1(d). We notice that the SDW gap does not exist along the whole k_y axis, although it opens at some k_y points[Fig. 1(d)]. Thus, the QSFs exhibit clear weights along the k_y axis, and the QPI pattern is dominated by the scattering processes along the k_y direction. It should be noted that at the center region around the Γ point the QPI pattern exhibits like a short dimer. However, it is not the substantial feature of the scattering pattern. When the energy is slightly away from $\omega = -0.14$, the short dimer diminishes but the vertical dimer structure remains. Actually, this dimer-like structure of the QPI pattern persists in the energy window of $-0.2 < \omega < -0.12$, which coincides basically with the energy region of the SDW gap in the single-particle spectrum as shown in Fig. 1(d). With the increase of energy, the pattern develops gradually into a broad peak around the Γ point and it has no obvious anisotropy as shown in Fig. 2(c) for $\omega = -0.08$. Moreover, the intensity of the QPI pattern is nearly three times larger than that with $\omega = -0.14$. This is the specific case in that this energy happens to be near the top of the hole band around (π, π) (not shown here), where the density of states is large and consequently the QSFs show a noticeable intensity around (π, π) as shown in Fig. 2(d). Above this energy region, one approaches gradually to the Fermi energy, so the QSFs will copy the main features of the FS. In this case, the QPI pattern is dominated by two sets of vertical dimers along the q_y direction as indicated by the q_1 and q_2 arrows in Fig. 2(e) for $\omega = -0.04$, which arises from the inter-hole-pocket and intra-hole-pocket scatterings, respectively [see Fig. 2(f)]. What we distinguish the two sets of vertical dimers comes from the features exhibited in the QSF shown in Fig. 2(f). From this figure, one can see that the contour of the QSF is elongated along the q_y direction, so that the portions of the contours connected by q_2 become more or less flat, and thus the scatterings across the vertical nearly flat portions are dominant and give rise to the vertical dimers. Actually, this kind of dimer structure of the QPI patterns persists in the energy regime of $-0.03 < \omega < -0.01$. In the positive energy regime, the dimer structure of the QPI pattern diminishes gradually. The typical QPI pattern is shown in Fig. 2(g) for $\omega = 0.08$, which is dominated by a peak around the Γ point. This is consistent with the QSFs analysis, where its anisotropy weakens significantly in the positive energy regime [Fig. 2(h)]. It is mainly because the energy band above the Fermi level is less distorted by the SDW formation, as can be seen from a comparison between Fig. 1(b) and (d). It was carefully

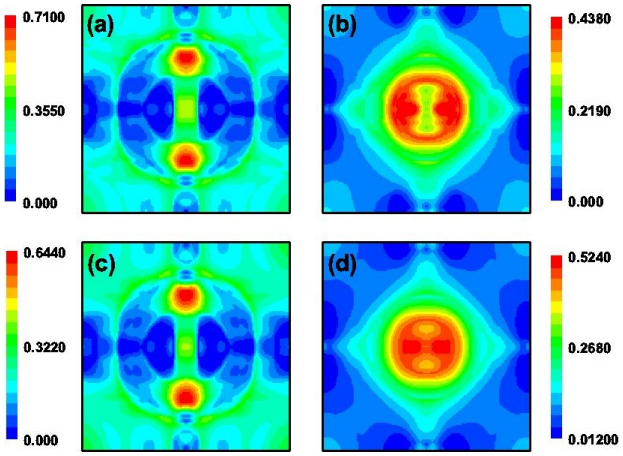

FIG. 3. (Color online) QPI patterns in the magnetically driven nematic phase. Panels (a) and (c) are the QPI patterns at $\omega = -0.14$ for $\xi = 80$ and $\xi = 20$, respectively. Panels (b), (d) are the QPI patterns at $\omega = -0.04$ for $\xi = 80$ and $\xi = 20$, respectively.

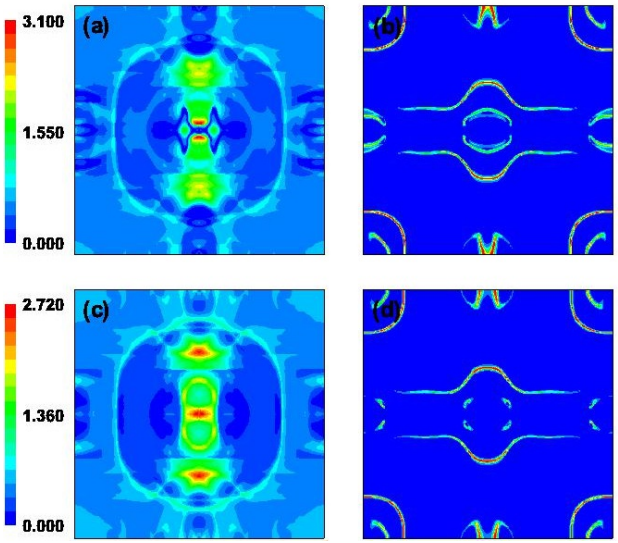

FIG. 4. (Color online) QPI patterns and intensity maps of QSFs in the SDW state with and without the off-diagonal SDW orders. Panels (a) and (c) are the QPI patterns for $\omega = -0.15$ without and with the off-diagonal SDW orders, respectively. The intensity maps of the corresponding QSFs are plotted in the right panels.

checked that the above mentioned features of the QPI patterns persist for weak impurity scattering regardless of the sign of V.

Theoretically, the features of the QPI patterns in the SDW state have been investigated by previous studies[37–39]. Similar to the results presented in Fig. 2(e) and (f), the highly anisotropic QPI patterns obtained by previous studies[37–39] are directly related to the topology of the SDW distorted constant energy contours. Here, we emphasize another cause leading to the dimer structure in QPI pattern, that is the highly anisotropic SDW gaps in the momentum space which is directly related to the orbital characters of the folded bands as addressed above.

In the magnetically driven nematic phase, the long-range SDW order gives way to the short-range antiferromagnetic correlation which is modelled by the Lee-Rice-Anderson formula[28] as introduced above. In this case, the magnetic correlation length ξ is the relevant parameter. Therefore, let us study the evolution of the QPI patterns with the reduction of the magnetic correlation length ξ. The QPI patterns for $\omega = -0.14$ are shown in Fig. 3(a) and (c) for $\xi = 80$ and $\xi = 20$, respectively. Compared to that with the SDW long-range order [Fig. 2(a)], the main feature still exhibits the anisotropy with the noticeable intensity of the pattern along the q_y direction. It is the consequence of the gap opening due to the short-range magnetic correlation similar to that in the SDW scenario discussed above. The variation is that two new peaks emerge at the two ends of the dimer-like structure. From Fig. 3(a) and (c), one can also see that this kind of QPI structure is less affected by the change of ξ from 80 to 20. We also notice that it preserves in the same energy window of $-0.2 < \omega < -0.12$ to the case of the SDW order. It is interesting to notice that similar QPI patterns have been experimentally observed in the ferropnictide 122 compounds[40], although the observed dimers are shorter. The results for $\omega = -0.04$ are presented in Fig. 3(b) and (d). It shows that the q_1 and q_2 dimers presented in the SDW state merge together to give rise to a loop around the Γ point when the correlation length is $\xi = 80$. The mergence becomes strongly with the further decreasing of ξ, and eventually a nearly flat-top broad peak around the Γ point will appear, as has already been seen from Fig. 3(d) for $\xi = 20$. Thus, it can be found that the anisotropy of the QPI patterns weakens significantly with the reduction of ξ. With a finite correlation length ξ, the SDW gives way to the damped spin excitations. The damping becomes stronger with the decrease of the correlation length ξ. As a result, the quasiparticle peak is broadened correspondingly due to its coupling to these damped spin excitations as indicated by the Lee-Rice-Anderson formula[28] used above, so do the main features of the QPI around the Γ point. In the case of $\omega = -0.14$, the dimer structure along the q_y direction in the SDW phase is mainly caused by the opening of the SDW gap along the k_x direction of the single-particle spectrum which is affected less by the quasiparticle damping. Thus, the anisotropic feature of the QPI pattern for $\omega = -0.14$ persists even when ξ is significantly reduced.

It was checked that the above mentioned features of the QPI patterns are qualitatively unchanged when the interacting parameters vary within a realistic region suggested in Ref.[26]. We have also considered the effects of the band structure on QPI patterns by using the LDA energy bands of LiFeAs[41–43]. It was found that the QPI patterns also exhibit the prominent dimer structure when

energy is in the SDW gap region. The dimers of the QPI patterns persist when the energy is around the Fermi level, and they weakens gradually with the reduction of the magnetic correlation length in the magnetic nematic phase. It should be noticed that there exist significant differences between the energy bands of LiFeAs and those of LaOFeAs[24,41,42]. Thus, the QPI features established above is robust.

Furthermore, it was checked that the main features of the QPI patterns remain when the off-diagonal SDW orders are considered. Here, we do not present detail comparisons between the QPI patterns with and without the off-diagonal SDW orders in all cases. Instead, we give a typical example to show the behaviors of the scattering patterns when the off-diagonal SDW orders are taken into account. We show the QPI patterns for $\omega = -0.15$ in Fig. 4(a) and (c) in the SDW state without and with the off-diagonal SDW orders, respectively. As shown in Fig. 4(a), the QPI pattern for $\omega = -0.15$ exhibits a dimer-like structure orienting along the q_y axis which is similar to that presented in Fig. 4(c) with the off-diagonal SDW orders, although some differences around the Γ point exists. This stems from the effect of the highly anisotropic SDW gaps in momentum space, which is less subjected to the inclusion of the off-diagonal SDW orders as shown by the QSFs in Fig. 4(b) and (d). We also note that there is an approximate 10% increase in magnitudes of the converged diagonal SDW orders after including the off-diagonal terms as presented in Sec.IIA. As a consequence, the QPI pattern shown in Fig. 4(c) for $\omega = -0.15$ has nearly the same structure as that shown in Fig. 2(a) for a slightly different energy of $\omega = -0.14$.

B. QPI patterns in the orbital scenario of nematicity

Experimentally, it was found that the degeneracy between the d_{xz} and d_{yz} bands is lifted at a temperature coincident with the onset of nematicity[6,8,12]. Theoretically, it was proposed[16,29,30] that the nematicity may originate from the orbital fluctuations. However, it is difficult to distinguish the orbital driven nematicity from its spin counterpart due to their mutual coupling[4]. In this section, we study the QPI patterns induced by the potential scattering in the orbital scenario of nematicity.

We note that it was recently revealed by ARPES experiments that the orbital order is strongly momentum dependent in FeSe[44,45]. With the help of the symmetry analysis, we will first obtain the general form of the orbital order up to the nearest-neighbor sites. In the present model, the point group of the Fe plane is $\{e, c_4^1, c_4^2, c_4^3, c_x, c_y, \sigma_+, \sigma_-\}$, where $c_4^n = (c_4^1)^n$ with c_4^1 a $\pi/2$ rotation along the z axis followed by a Fe plane mirror reflection, c_x and c_y are π rotations along the x and y axis of the Fe-Fe bond, respectively. σ_+ and σ_- are two mirrors determined by the nearest-neighbor Fe and As atoms, respectively. It was found experimentally that the Dirac cone dispersion exists in the SDW state[46]. As pointed out by previous study[31], the emergence of the Dirac cones is a consequence of the c_x and c_y symmetries. In this way, we expect that the c_x and c_y symmetries are preserved in the SDW state. As proposed theoretically[14–17], the SDW state is expected to occur as a result of the spontaneous symmetry breaking of the nematic phase. Thus, the c_x and c_y symmetries are preserved in the nematic phase. This is further supported by recent ARPES observations[47,48]. In this way, the point group of the nematic phase is $\{e, c_4^2, c_x, c_y\}$. Generally, the Hamiltonian for the orbital order can be written as $H_{orb} = \sum_{ij,ab,\sigma} \lambda_{ij,ab} C^+_{ia\sigma} C_{jb\sigma}$, where i, j and a, b are the lattice sites and orbital indices, respectively. Considering the point group symmetry and that the t_{2g} orbitals dominate the low energy electronic bands, we find that the H_{orb} with only the on-site orbital order reads $\sum_{i,\sigma} \lambda_0 (C^+_{i\sigma,xz} C_{i\sigma,xz} - C^+_{i\sigma,yz} C_{i\sigma,yz})$. Other terms, such as $\sum_{i\sigma} C^+_{i\sigma,xz} C_{i\sigma,yz}$, are forbidden since they break the c_x and c_y symmetries. The H_{orb} with the orbital orders up to the nearest-neighbor sites are written as $\sum_{k\sigma} \lambda_0 (C^+_{k\sigma,xz} C_{k\sigma,xz} - C^+_{k\sigma,yz} C_{k\sigma,yz}) + \lambda_1 (\cos k_x + \cos k_y)(C^+_{k\sigma,xz} C_{k\sigma,xz} - C^+_{k\sigma,yz} C_{k\sigma,yz}) + \lambda_2 (\cos k_x - \cos k_y)(C^+_{k\sigma,xz} C_{k\sigma,xz} + C^+_{k\sigma,yz} C_{k\sigma,yz}) + i\lambda_3 \sin k_x C^+_{k\sigma,xy} C_{k\sigma,xz} - i\lambda_3 \sin k_y C^+_{k\sigma,xy} C_{k\sigma,yz} + h.c. + \lambda_4 (\cos k_x - \cos k_y) C^+_{k\sigma,xy} C_{k\sigma,xy}$. We can of course construct the orbital orders up to the next-nearest-neighbor sites in a similar way, however, this introduces more parameters which complicate the problem. In general, the magnitude of the order will decrease with the increase of the lattice distance. So, we will focus on the orbital orders up to the nearest-neighbor sites which are believed to have captured the main physics.

1. *orbital order with momentum dependence*

We use the above obtained Hamiltonian for the orbital orders to fit the splitting energy between the d_{xz} and d_{yz} bands observed in experiments[44,45]. Experimentally, the splitting at Γ point is about 0.02, and that between the d_{yz} band at X point and the d_{xz} band at Y point is increased to be 0.08. The parameters are $\lambda_0 = 0.01, \lambda_1 = 0, \lambda_2 = 0.015, \lambda_3 = 0.005, \lambda_4 = 0.002$, which can reproduce the experimental data well. The resulted energy bands are shown in Fig. 5(a). The outer hole band along the $(0,0) - (\pi,0)$ direction is mainly of the d_{yz} orbital character, while that along the $(0,0) - (0,\pi)$ direction is of d_{xz} character.

Let us first discuss the effects on the energy band due to the orbital orders. Because the outer hole band and the electron band along the k_x axis are even and odd parities under the c_x operation. As a result, no gap opens at the intersection point $(0.84\pi, 0)$ between the outer hole band and the electron band. It leads to a Dirac cone dispersion around $(\pi, 0)$. Equivalently, there exists another Dirac cone band around $(0, \pi)$. The locations of the two

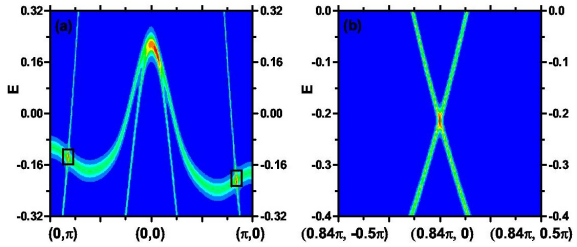

FIG. 5. (Color online) (a) Energy bands along the high symmetry directions in the presence of momentum dependent orbital order. The outer hole band along the $(0,0)-(\pi,0)$ and $(0,0)-(0,\pi)$ directions are mainly composed of the d_{yz} and d_{xz} orbitals, respectively. The two black squares mark the location of the two Dirac nodes which reside on the k_x and k_y axes. (b) Linear dispersion for the Dirac cone located at k_x axis. This panel is plotted along the $(0.84\pi, k_y)$ line. The Dirac node locates at $(0.84\pi, 0)$.

Dirac points are marked by the black squares in Fig. 5(a). These two Dirac cones are inequivalent in energy due to the C_4 symmetry breaking induced by the orbital orders. The node energies are $\omega_x = -0.21$ and $\omega_y = -0.14$ for the Dirac cones located at the k_x and k_y axes, respectively. In Fig. 5(b), we show the dispersion of the low energy Dirac cone at $(0.84\pi, 0)$ along the $(0.84\pi, k_y)$ direction. It is interesting to notice that the similar cone like dispersion has been observed by the recent ARPES measurements on thin FeSe films[47,48], although the observed Dirac cone is just below the Fermi level. On the other hand, compared to the complicated energy bands reconstruction induced by the SDW order as shown in Fig. 1(c), the distorted energy bands due to the orbital orders are dominated by two hole bands around the Γ point and two electron bands around the $(\pi, 0)$ and $(0, \pi)$ points.

Now, we turn to the study of the energy evolution of the QPI patterns in the orbital scenario of nematicity. The results are obtained in a wide energy window from $\omega = -0.3$ to $\omega = 0.3$, and the anisotropy of the QPI pattern is rather weak when $\omega > -0.06$ suggesting that it is irrelevant to the orbital orders above this energy. Thus, we show the typical patterns in Fig. 6 (a), (c), and (e) for $\omega = -0.24$, -0.18 and -0.1, respectively. For $\omega = -0.24$, the scattering pattern is highly anisotropic with its main intensity along the q_x axis, leading to a horizontal dimer. When the energy is increased to be near $\omega = -0.18$, the QPI pattern turns to be a vertical dimer. This vertical dimer remains up to a higher energy $\omega = -0.1$ which is slightly above ω_y, although additional structures develop around the dimer. With the further increasing of energy, the anisotropy of the QPI patterns weakens significantly. Especially, the scattering patterns exhibit little anisotropy in the positive energy region.

The transition of the QPI patterns from the horizontal to vertical structure is associated with the inequivalent energy positions of the two Dirac cones due to the C_4 symmetry breaking induced by the orbital orders. As

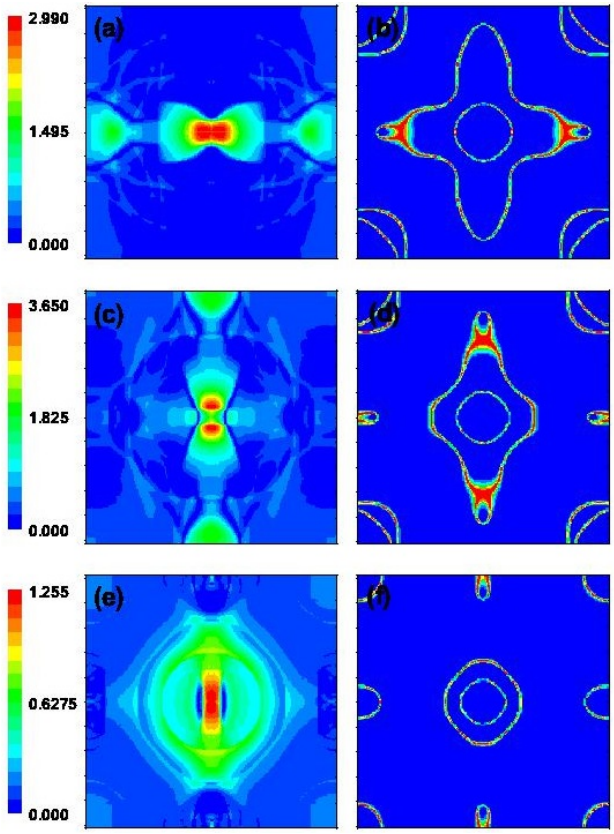

FIG. 6. (Color online) Energy evolution of the QPI patterns in the orbital driven nematic phase with strongly momentum dependent orbital order. Left panels are the QPI patterns for $\omega = -0.24$, -0.18 and -0.1, respectively. Right panels are the intensity map of the corresponding quasiparticle spectral functions.

shown in Fig. 6(b), (d) and (f), the spectral function shows a large intensity around the Dirac cones. It attributes to the small velocity of the outer d_{yz} and d_{xz} bands around the two Dirac cones. So, the QPI process is dominated by the Dirac cone to Dirac cone scatterings of quasiparticles. For $\omega = -0.24$, the nearby Dirac cones situate at the k_x axis. But, for $\omega = -0.18$ and -0.1, they situate at the k_y axis. So, the Dirac cone to Dirac cone scatterings lead to the transition of the QPI patterns which is related to the presence of the orbital orders.

2. *orbital order without momentum dependence*

Though the orbital order is momentum dependent in FeSe[44,45], this may vary in different kinds of IBSCs. As a comparison, we will study the energy evolution of the QPI patterns with a momentum independent orbital order in this section. The parameters $\lambda_0 = 0.04, \lambda_{1,2,3,4} = 0$ give rise to a momentum independent orbital order as that used in previous studies[29,30]. As shown in Fig. 7(a), the resulted energy splitting between the d_{xz} and d_{yz}

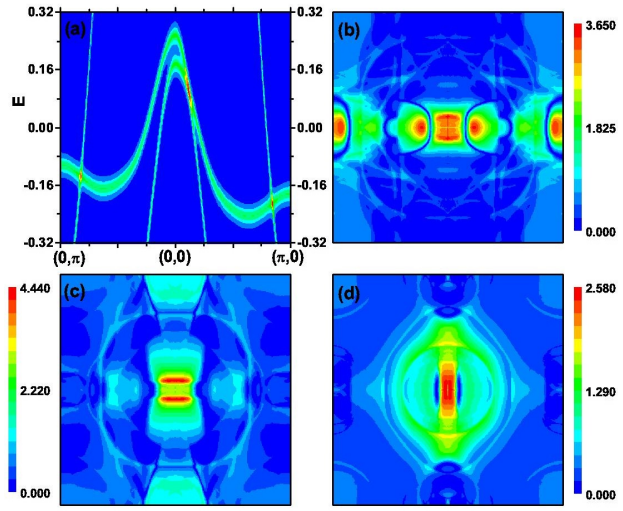

FIG. 7. (Color online) Energy bands reconstruction and the energy evolution of the QPI patterns in the orbital driven nematic phase with the momentum independent orbital order. Panel (a) is the energy bands along the high symmetry direction. The outer hole bands along the $(0,0)-(\pi,0)$ and $(0,0)-(0,\pi)$ directions are mainly of the d_{yz} and d_{xz} characters, respectively. Panels (b), (c) and (d) are the QPI patterns for $\omega=-0.24$, -0.18 and -0.1, respectively.

bands are 0.08 at Γ. And it has the same splitting energy between the d_{xz} band around Y and the d_{yz} band around X. The magnitude of this splitting energy is comparable to that obtained by the ARPES experiments[12,35].

To make a comparison to the results for the momentum dependent orbital order, we present the QPI patterns at $\omega=-0.24$, -0.18, and -0.1 in Fig. 7(b)-(d). Quite similarly, the main feature of the QPI patterns exhibits a transition from the horizontal dimer at a low energy $\omega=-0.24$ to the vertical dimer at $\omega=-0.18$, and the vertical dimer persists up to a high energy $\omega=-0.1$. It should be noticed that the horizontal dimers with the highest intensity in Fig. 7(c) are not the substantial feature of the QPI pattern due to the fact that they diminish when the energy is away from $\omega=-0.18$. It is carefully checked that the main features of the QPI patterns keep unchanged when the orbital orders evolve smoothly from the strongly momentum dependent case to the momentum independent case, if the splitting energy between the d_{xz} band at Y and the d_{yz} band at X is fixed to be 0.08. Thus, the above established transition of the QPI patterns is a robust phenomenon, regardless of the momentum dependence of the orbital orders. The difference in the energy splitting of the d_{xz} and d_{yz} bands between the momentum dependent and independent orbital orders is that there is a constant energy splitting in the latter case. Thus, the two Dirac cones that situate near the $(\pi,0)$ and $(0,\pi)$ points are not affected by the difference of the momentum dependence of the orbital order as shown clearly in Fig. 5(a) and Fig. 7(a). Thus, the main feature of the QPI patterns is unchanged because it mainly arises from the Dirac cones to Dirac cones scatterings.

Before concluding Sec.IIIB, it is worth mentioning that the transition of the QPI patterns is related to the C_4 symmetry breaking induced by the orbital order and the parities of relative bands which are both involved with the symmetry of the orbital nematic phase. Thus it is expected that the above established transition remains unchanged when the interactions between electrons are taken into account. Actually, there exists numerical evidence[49] that the symmetries of relative bands do not change when the correlation effects are considered. We also note that the established transition of QPI patterns occurs at energies much below the Fermi level. Considering that the bandwidth is significantly reduced when the Coulomb interactions are taken into account[49–52], we expect that the energy difference between the transition and the Fermi level will be reduced and it will facilitate the experimental measurements. On the other hand, it was experimentally found on the FeSe films that the Dirac cones reside slightly below the Fermi level[47,48]. This indicates that the transition of QPI patterns can be observed at energies close to the Fermi level in some iron pnictides, at least in the FeSe films.

IV. SUMMARY AND DISCUSSION

In conclusion, we have studied theoretically the quasiparticle scattering interference patterns in the nematic phase of the iron-based superconductors based on the magnetic and orbital scenarios, respectively.

Deep in the SDW state, the QPI patterns exhibit a dimer structure in a wide energy region and develop a bi-dimer structure when the energy is increased to be near the Fermi level. It is also shown that the dimer structure of the QPI patterns still exists when the SDW state is replaced by the state with fluctuating magnetic order, though the bi-dimer structure is smeared due to the mergence of the two sets of dimers when the short-range correlation length is significantly decreased.

Thus, we identify that the QPI dimers present in the SDW and the magnetic nematic phase orient along the ferromagnetic direction of the SDW order as long as the correlation length is not significantly decreased. Our results based on the magnetic scenario of nematicity are qualitatively consistent with the STM observations on NaFeAs[22].

In the orbital scenario of nematicity, the QPI patterns are dominated by a dimer structure along the q_x or q_y axes in a wide energy region. A $\pi/2$ rotation of the dimer structure occurs when the energy increases from the lower Dirac node to the higher one. Above the two Dirac nodes, the anisotropy of the QPI patterns is significantly weakened. Furthermore, it is found that this transition is insensitive to the momentum dependence of the orbital order.

Theoretically, the suggestions for distinguishing the

SDW order from the orbital driven nematicity by using STM technique have been proposed[53,54]. Plonka *et al.*[53] focus on the contributions of the band extrema (local maxima or minima in the bands) to the local density of states (LDOS) and QPI. They found that the features related to the differences between two band extrema which track the orbital splitting or the SDW gap can be used to distinguish between the orbital splitting and the SDW order. The features are easy to be detected in LDOS, but are obscured in QPI by contributions from orbitals other than d_{xz} and d_{yz}. Eremin *et al.*[54] focus on the QPI at an energy near the Fermi level, so the anisotropic QPI patterns are closely related to the topology of the SDW or orbital order distorted constant energy contours near the Fermi level. Here, we uncover the significant contributions to QPI from the Dirac cone to Dirac cone scatterings of quasiparticles in the orbital scenario. For the magnetic scenario, we elaborate the robust dimer structure in QPI patterns resulting from the highly anisotropic SDW gaps in the momentum space which are directly related to the orbital characters of the folded bands. We further show that due to the inequivalent energies of the two Dirac nodes, the dimer structure in the orbital scenario undergoes a $\pi/2$ rotation with the increase of energy, which contrasts clearly with the case of the magnetic scenario. These features of the QPI patterns have not been addressed in previous studies[37–39,53,54]. In addition, compared to Ref.[54] in which the two-orbital model is used, we carry out the calculations by using the more realistic five-orbital model.

From the results presented in this paper, we conclude that the QPI patterns exhibit dimer structure in a wide energy region in both the magnetic and the orbital scenarios of nematicity. The dimer tends to orient along the ferromagnetic direction in the magnetic case. However, it undergoes a $\pi/2$ rotation with the increase of energy in the orbital case. Thus, our results established in this paper for the QPI patterns may be used to probe the origin of nematicity in various iron-based superconductors.

V. ACKNOWLEDGEMENT

This work was supported by the National Natural Science Foundation of China (11190023 and 11374138), and National Key Projects for Research & Development of China (Grant No. 2016YFA0300401).

* jxli@nju.edu.cn

[1] C. R. Rotundu, and R. J. Birgeneau, Phys. Rev. B **84**, 092501 (2011).

[2] S. Avci, O. Chmaissem, D. Y. Chung, S. Rosenkranz, E. A. Goremychkin, J. P. Castellan, I. S. Todorov, J. A. Schlueter, H. Claus, A. Daoud-Aladine, D. D. Khalyavin, M. G. Kanatzidis, and R. Osborn, Phys. Rev. B **85**, 184507 (2012).

[3] L. Ma, J. Dai, P. S. Wang, X. R. Lu, Y. Song, C. L. Zhang, G. T. Tan, P. C. Dai, D. Hu, S. L. Li, B. Normand, and W. Q. Yu, Phys. Rev. B **90**, 144502 (2014).

[4] R. M. Fernandes, A. V. Chubukov, and J. Schmalian, Nat. Phys. **10**, 97 (2014).

[5] S. Kasahara, H. J. Shi, K. Hashimoto, S. Tonegawa, Y. Mizukami, T. Shibauchi, K. Sugimoto, T. Fukuda, T. Terashima, A. H. Nevidomskyy, and Y. Matsuda, Nature **486**, 382 (2012).

[6] H. Miao, L. M. Wang, P. Richard, S. F. Wu, J. Ma, T. Qian, L. Y. Xing, X. C. Wang, C. Q. Jin, C. P. Chou, Z. Wang, W. Ku, and H. Ding, Phys. Rev. B **89**, 220503(R) (2014).

[7] J. J. Wu, J. F. Lin, X. C. Wang, Q. Q. Liu, J. L. Zhu, Y. M. Xiao, P. Chow, and C. Q. Jina, Proc. Natl. Acad. Sci, USA **110**, 17263 (2013).

[8] K. Nakayama, Y. Miyata, G. N. Phan, T. Sato, Y. Tanabe, T. Urata, K. Tanigaki, and T. Takahashi, Phys. Rev. Lett. **113**, 237001 (2014).

[9] J. H. Chu, J. G. Analytis, K. D. Greve, P. L. McMahon, Z. Islam, Y. Yamamoto, I. R. Fisher, Science **329**, 824 (2010).

[10] M. A. Tanatar, E. C. Blomberg, A. Kreyssig, M. G. Kim, N. Ni, A. Thaler, S. L. Budko, P. C. Canfield, A. I. Goldman, I. I. Mazin, and R. Prozorov, Phys. Rev. B **81**, 184508 (2010).

[11] X. Y. Lu, J. T. Park, R. Zhang, H. Q. Luo, A. H. Nevidomskyy, Q. M. Si, P. C. Dai, Science **345**, 657 (2014).

[12] T. Shimojima, T. Sonobe, W. Malaeb, K. Shinada, A. Chainani, S. Shin, T. Yoshida, S. Ideta, A. Fujimori, H. Kumigashira, K. Ono, Y. Nakashima, H. Anzai, M. Arita, A. Ino, H. Namatame, M. Taniguchi, M. Nakajima, S. Uchida, Y. Tomioka, T. Ito, K. Kihou, C. H. Lee, A. Iyo, H. Eisaki, K. Ohgushi, S. Kasahara, T. Terashima, H. Ikeda, T. Shibauchi, Y. Matsuda, and K. Ishizaka, Phys. Rev. B **89**, 045101 (2014).

[13] T. Iye, M. H. Julien, H. Mayaffre, M. Horvatić, C. Berthier, K. Ishida, H. Ikeda, S. Kasahara, T. Shibauchi, and Y. Matsuda, J. Phys. Soc. Jpn. **84**, 043705 (2015).

[14] C. Fang, H. Yao, W. F. Tsai, J. P. Hu, and S. A. Kivelson, Phys. Rev. B **77**, 224509 (2008).

[15] C. K. Xu, M. Müller, and S. Sachdev, Phys. Rev. B **78**, 020501(R) (2008).

[16] H. Kontani, T. Saito, and S. Onari, Phys. Rev. B **84**, 024528 (2011).

[17] R. M. Fernandes, A. V. Chubukov, J. Knolle, I. Eremin, and J. Schmalian, Phys. Rev. B **85**, 024534 (2012).

[18] J. E. Hoffman, K. McElroy, D. H. Lee, K. M. Lang, H. Eisaki, S. Uchida, J. C. Davis, Science **297**, 1148 (2002).

[19] Q. H. Wang, D. H. Lee, Phys. Rev. B **67**, 020511 (2003).

[20] W. C. Lee, and C. Wu, Phys. Rev. Lett. **103**, 176101 (2009).

[21] W. C. Lee, D. P. Arovas, and C. Wu, Phys. Rev. B **81**, 184403 (2010).

[22] E. P. Rosenthal, E. F. Andrade, C. J. Arguello, R. M. Fernandes, L. Y. Xing, X. C. Wang, C. Q. Jin, A. J. Millis, and A. N. Pasupathy, Nat. Phys. **10**, 225 (2014).

[23] P. Cai, W. Ruan, X. D. Zhou, C. Ye, A. F. Wang, X. H. Chen, D. H. Lee, and Y. Y. Wang, Phys. Rev. Lett. **112**,

127001 (2014).
[24] S. Graser, T. A. Maier, P. J. Hirschfeld, and D. J. Scalapino, New J. Phys. **11**, 025016 (2009).
[25] E. Bascones, M. J. Calderón, and B. Valenzuela, Phys. Rev. Lett. **104**, 227201 (2010).
[26] Q. L. Luo, G. Martins, D. X. Yao, M. Daghofer, R. Yu, A. Moreo, and E. Dagotto, Phys. Rev. B **82**, 104508 (2010).
[27] M. N. Gastiasoro, and B. M. Andersen, J. Supercond. Novel Magn. **26**, 2651 (2013).
[28] P. A. Lee, T. M. Rice, and P. W. Anderson, Phys. Rev. Lett. **31**, 462 (1973).
[29] C. C. Chen, J. Maciejko, A. P. Sorini, B. Moritz, R. R. P. Singh, and T. P. Devereaux, Phys. Rev. B **82**, 100504(R) (2010).
[30] W. C. Lv, and P. Phillips, Phys. Rev. B **84**, 174512(R) (2011).
[31] Y. Ran, F. Wang, H. Zhai, A. Vishwanath, and D. H. Lee, Phys. Rev. B **79**, 014505 (2009).
[32] P. Richard, K. Nakayama, T. Sato, M. Neupane, Y. M. Xu, J. H. Bowen, G. F. Chen, J. L. Luo, N. L. Wang, X. Dai, Z. Fang, H. Ding, and T. Takahashi, Phys. Rev. Lett. **104**, 137001 (2010).
[33] C. He, Y. Zhang, B. P. Xie, X. F. Wang, L. X. Yang, B. Zhou, F. Chen, M. Arita, K. Shimada, H. Namatame, M. Taniguchi, X. H. Chen, J. P. Hu, and D. L. Feng, Phys. Rev. Lett. **105**, 117002 (2010).
[34] M. Yi, D. H. Lu, J. H. Chu, J. G. Analytis, A. P. Sorini, A. F. Kemper, B. Moritz, S. K. Mo, R. G. Moore, M. Hashimoto, W. S. Lee, Z. Hussain, T. P. Devereaux, I. R. Fisher, and Z. X. Shen, Proc. Natl. Acad. Sci, USA **108**, 6878 (2011).
[35] Y. Zhang, C. He, Z. R. Ye, J. Jiang, F. Chen, M. Xu, Q. Q. Ge, B. P. Xie, J. Wei, M. Aeschlimann, X. Y. Cui, M. Shi, J. P. Hu, and D. L. Feng, Phys. Rev. B **85**, 085121 (2012).
[36] M. N. Gastiasoro, and B. M. Andersen, Phys. Rev. B **92**, 140506 (2015).
[37] J. Knolle, I. Eremin, A. Akbari, and R. Moessner, Phys. Rev. Lett. **104**, 257001 (2010).
[38] A. Akbari, J. Knolle, I. Eremin, and R. Moessner, Phys. Rev. B **82**, 224506 (2010).
[39] I. I. Mazin, S. A. J. Kimber, and D. N. Argyriou, Phys. Rev. B **83**, 052501 (2011).
[40] T. M. Chuang, M. P. Allan, J. Lee, Y. Xie, Ni Ni, S. L. Bud'ko, G. S. Boebinger, P. C. Canfield, J. C. Davis, Science **327**, 181 (2010).
[41] Y. Wang, A. Kreisel, V. B. Zabolotnyy, S. V. Borisenko, B. Büchner, T. A. Maier, P. J. Hirschfeld, and D. J. Scalapino, Phys. Rev. B **88**, 174516 (2013).
[42] F. Ahn, I. Eremin, J. Knolle, V. B. Zabolotnyy, S. V. Borisenko, B. Büchner, and A. V. Chubukov, Phys. Rev. B **89**, 144513 (2014).
[43] M. N. Gastiasoro, P. J. Hirschfeld, and B. M. Andersen, Phys. Rev. B **88**, 220509 (2013).
[44] P. Zhang, T. Qian, P. Richard, X. P. Wang, H. Miao, B. Q. Lv, B. B. Fu, T. Wolf, C. Meingast, X. X. Wu, Z. Q. Wang, J. P. Hu, and H. Ding, Phys. Rev. B **91**, 214503 (2015).
[45] Y. Zhang, M. Yi, Z. K. Liu, W. Li, J. J. Lee, R. G. Moore, M. Hashimoto, N. Masamichi, H. Eisaki, S. K. Mo, Z. Hussain, T. P. Devereaux, Z. X. Shen, D. H. Lu, arXiv:**1503**. 01556 (2015).
[46] P. Richard, K. Nakayama, T. Sato, M. Neupane, Y. M. Xu, J. H. Bowen, G. F. Chen, J. L. Luo, N. L. Wang, X. Dai, Z. Fang, H. Ding, and T. Takahashi, Phys. Rev. Lett. **104**, 137001 (2010).
[47] S. Y. Tan, Y. Fang, D. H. Xie, W. Feng, C. H. P. Wen, Q. Song, Q. Y. Chen, W. Zhang, Y. Zhang, L. Z. Luo, B. P. Xie, X. C. Lai, and D. L. Feng, Phys. Rev. B **93**, 104513 (2016).
[48] W. Li, Y. Zhang, J. J. Lee, H. Ding, M. Yi, Z. Li, P. Deng, K. Chang, S. K. Mo, M. Hashimoto, D. H. Lu, X. Chen, R. G. Moore, Q. K. Xue, and Z. X. Shen, arXiv:**1509**. 01892 (2015).
[49] J. Ferber, K. Foyevtsova, R. Valentí, and H. O. Jeschke, Phys. Rev. B **85**, 094505 (2012).
[50] M. Aichhorn, L. Pourovskii, V. Vildosola, M. Ferrero, O. Parcollet, T. Miyake, A. Georges, and S. Biermann, Phys. Rev. B **80**, 085101 (2009).
[51] Z. P. Yin, K. Haule, and G. Kotliar, Nat. Mat **10**, 932 (2011).
[52] P. Werner, M. Casula, T. Miyake, F. Aryasetiawan, A. J. Millis, and S. Biermann, Nat. Phys. **8**, 331 (2012).
[53] N. Plonka, A. F. Kemper, S. Graser, A. P. Kampf, and T. P. Devereaux, Phys. Rev. B **88**, 174518 (2013).
[54] I. Eremin, J. Knolle, R. M. Fernandes, J. Schmalian, and A. V. Chubukov, J. Phys. Soc. Jpn. **83**, 061015 (2014).